Springer

KSME

Journal of Mechanical Science and Technology 32 (5) (2018) 2069~2078
www.springerlink.com/content/1738-494x(Print)/1976-3824(Online)
DOI 10.1007/s12206-018-0416-1

Analysis of transient flow in a pump-turbine during the load rejection process †

Xiaolong Fu[1], Deyou Li[1,2,*], Hongjie Wang[1,*], Guanghui Zhang[1], Zhenggui Li[1,2] and Xianzhu Wei[1,3]

[1]*School of Energy Science and Engineering, Harbin Institute of Technology, Harbin 150001, China*
[2]*Key Laboratory of Fluid and Power Machinery (Xihua University), Ministry of Education Sichuan, Chengdu, 610039, China*
[3]*State Key Laboratory of Hydro-Power Equipment, Harbin Institute of Large Electrical Machinery, Harbin 150040, China*

(Manuscript Received August 26, 2017; Revised February 7, 2018; Accepted February 15, 2018)

Abstract

The transient flow in pump-turbines during the load rejection process is very complex. However, few studies have been conducted on three-dimensional (3-D) numerical simulation. Hence, we simulated 3-D transient turbulent flow in a pump-turbine during the load rejection process using the calculation method of coupling the flow with the rotor motion of rigid body. To simulate the unsteady boundary conditions, the dynamic closing process of the guide vanes was simulated with the dynamic mesh technology. The boundary conditions at the spiral-casing inlet and the draft tube outlet were determined using the user defined functions (UDF) according to the experimental data. The numerical results of the rotational speeds show a good agreement with the experimental data. Then, the complex transient flow in the pump-turbine during the load rejection process was analyzed based on the numerical results. The results show that there are severe unsteady vortex flows in the vaneless space near the conditions under which the hydraulic torque on the runner equals to zero. When the pump-turbine operates into the maximum reverse discharge condition in the reverse pump operating process, the unsteady vortex flows in the vaneless space are instantaneously impacted into the region between the guide vanes and the stay vanes by the sudden reverse flows. The formation and development mechanism of the unsteady vortex flow in the vaneless space is associated with the distribution characteristic of the velocity field.

Keywords: Pump-turbine; Load rejection process; Numerical simulation; Flow analysis; Unsteady vortex flow

1. Introduction

To promote sustainable development of energy resources, the problem of the power storage needs to be solved. The technology of pumped storage power generation is an effective approach to solve the problem of storage power [1, 2]. In recent years, the technology of the pumped storage power generation has been developing rapidly [3-5]. Pump turbines, as the key components of pumped storage power plants, constantly experience transitional processes between different operating regimes [6, 7]. Many related investigations in hydraulic machinery have been conducted. The existing investigations are mainly about three aspects: Numerical methods, dynamic instability, and special flows during the transient processes [8-10]. However, there has still not been a very clear recognition of the transient process of pump turbines.

To investigate the transient processes of hydraulic turbines with the method of the computational fluid dynamics (CFD), different numerical methods of the transient flow in hydraulic turbines during the transient processes have been explored. In the early phase, the transient processes of hydropower stations were simulated with the simplified one-dimensional (1-D) method [11]. Later, with the improvement of the computer resources, a full 3-D turbulent simulation method was proposed and used to simulate the transient flow in the entire flow passage of the pumped storage power plant from the upstream reservoir to the downstream reservoir during the pump power failure process [12]. The 3-D simulation method is feasible to predict the transient processes in engineering [13]. To determine the unsteady boundary condition at the draft tube inlet, Ruprecht et al. [14] presented a 1-D and 3-D coupling method. Then, Huang et al. [15] compared the above three kinds of simulation results of the load rejection process. The comparison results indicate that it is effective to capture the interaction between the transient flow in penstocks and the unsteady turbulent flow in pump-turbines using the1-D and 3-D coupling method. In addition, the dynamic instability and hysteresis could be captured through the1-D and 3-D coupling method [16]. Furthermore, considering the hydraulic acoustic characteristic in the transient process, a density function was introduced to calculate the compressibility of water in pump turbines during the load rejection process [17]. Considering the influence of unsteady boundary conditions on the accuracy

*Corresponding author. Tel.: +86 15244604600, Fax.: +86 45186413251
E-mail address: lideyou@hit.edu.cn, wanghongjie@hit.edu.cn
† Recommended by Associate Editor Weon Gyu Shin

of numerical simulation, Li et al. [18, 19] explored a new 3-D simulation method, in which the inlet and outlet boundary conditions are determined using the available experimental data. The studies indicate that the numerical method has the potential to facilitate both exploration and diagnosis of faults in hydraulic machines during transient operations.

Based on the existing numerical and experimental methods, the dynamic instabilities of hydraulic turbines during different transient processes were investigated in-depth. Some related experimental studies indicate the pressure fluctuations are very severe [20]. A significant dynamic loop characteristic and the dynamic instability could be observed during some transient processes [21-23]. To analyze the formation mechanism of the dynamic instability deeply during the transient process using the numerical method, numerous transient simulations were performed. Stens and Riedelbauch [24, 25] pointed out that the severe pressure fluctuations on the blades were associated with the rotating stall at the pressure sides of the runner blades and the unstable vortex rope in the draft tube. Through the 1-D and 3-D coupling simulation, the dynamic characteristic of pump-turbines was attributed to the successive characteristic of the flow patterns in the runaway process [26]. Additionally, Pavesi et al. [27] simulated the transient flow in a two-stage pump-turbine during the pumping power reduction process. The results indicate that the hump characteristic of the pump-turbine was caused by two 3-D unsteady flow structures in the return channel and the wicket gates at the end of the first stage. Fan et al. [28] investigated the relationships between vibrations, noises and flow states in a pump-turbine during the process of start-up and shutdown in turbine mode and pointed out that the vibrations and noises of the distributor within the slight opening were caused by the repeated reversal of the fluid.

It can be seen that the unstable and unsteady flows in hydraulic turbines are the crucial reasons causing the dynamic instability. Therefore, there are many studies on the internal special flows in different type hydraulic turbines during the transient processes. For the bulb hydraulic turbine, there appears the reflux at the entrance of the runner and severe vortex phenomenon in the guide vanes and the draft tube during the load rejection process [29]. For the Francis turbine, there are some complex flow behaviors, including the flow separation vortex and back flow in the runner and the draft tube during the load rejection [30, 31]. For the model Kaplan turbine, the swirling flows in the draft tube become more severe in the latter part of the runaway process, which cause pressure fluctuations and even threaten the stability of the hydropower system considerably [32]. For the pump-turbine, there exists a strong interaction among different flow patterns in the vaneless space from no-load conditions into the S-shaped in the transient mode [33].

At present, most investigations on the transient process are about the numerical method, the dynamic instability of hydraulic turbines and the special flows in the draft tube during the transient processes. The deep investigations on the flow in the transient processes are mostly about the special flows in the draft tube. There are few studies focusing on the complex transient flow and its formation mechanism in the runner and the guide/stay vanes. Therefore, we analyzed the development process and its formation mechanism of the complex transient flow in the runner and the guide/stay vanes in detail.

First, we established reasonable boundary conditions based on the existing experimental data of the pump-turbine during the load rejection process. Secondly, the transient flow in the pump-turbine was simulated during the load rejection process. The simulated rotational speeds were compared with the corresponding experimental data. According to the numerical results of the pump-turbine during the load rejection process, the development process of the transient flow in the guide/stay vanes and the runner was analyzed with different methods. Finally, the formation mechanism of the complex transient flow in the guide/stay vanes and the runner was analyzed using the simplified transport equation of vorticity.

Table 1. Parameters of prototype pump-turbine (turbine mode).

Parameters	Value
Nominal diameter of runner at inlet (mm)	4850
Nominal diameter of runner at outlet (mm)	2535
Number of runner blades	9
Number of stay vanes	20
Number of guide vanes	20
The height of guide vane (mm)	425
Guide vane rated opening (degree)	20.69
Turbine mode rated head (m)	447
Turbine mode rated discharge (m^3/s)	96.34
Turbine mode rated speed (r/min)	375

2. Computational model and numerical method

2.1 Computational domain

The investigated pump-turbine comes from a real pumped storage power plant in China. Its basic parameters are listed in Table 1. The size of the prototype is scaled to the size of the reduced model (1:9.24). The nominal diameter at the inlet of the model runner is 274 mm.

The entire computational domain consists of the spiral-casing, the stay vanes, the guide vanes, the runner, the draft tube and the clearance between the runner and the stationary parts including the cover and the bottom ring as shown in Figs. 1 and 2.

2.2 Grid generation

The structural grids were generated in all computational domains except the guide vanes. To simulate the dynamic closing process of the guide vanes with the dynamic mesh technology, the 2.5 dimensional hybrid grids were generated

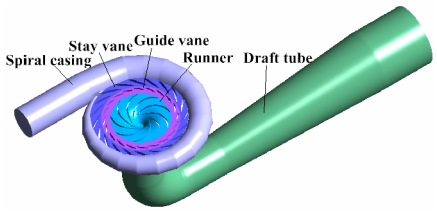

Fig. 1. Computational domain.

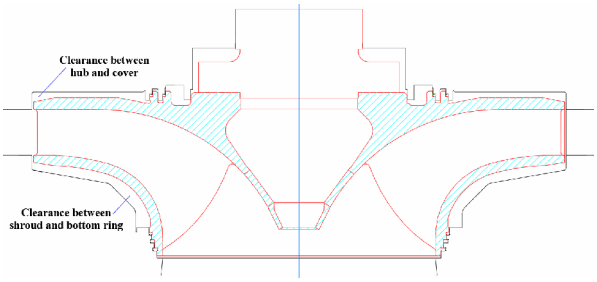

Fig. 2. Clearance between the runner and the stationary parts.

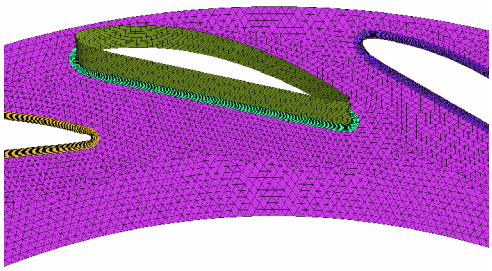

Fig. 3. Grids in the guide vanes.

in the guide vanes as shown in Fig. 3.

2.3 Grid independency verification

We generated seven sets of grids, whose numbers of nodes are from five million to eight million, in the whole computational domain with a 25 mm guide vane opening. The steady flow in the pump-turbine was simulated with the pressure boundary conditions at the spiral casing inlet and the draft tube outlet. The relationship between the discharge and the number of computational nodes is shown in Fig. 4. Considering the accuracy and the available computer resources, the grid with 7.27 million computational nodes was selected to calculate the transient flow in the pump-turbine during the load rejection process.

2.4 Boundary conditions

All the boundary conditions were established according to the dynamic experimental data and related operating data of the pumped storage power plant. The unsteady total pressure and static pressure boundary conditions were determined, respectively, at the inlet of the spiral-casing and the outlet of

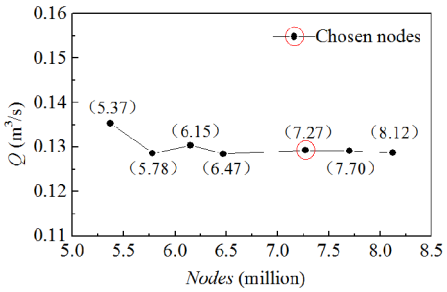

Fig. 4. Relationship between the discharge and the number of computational nodes.

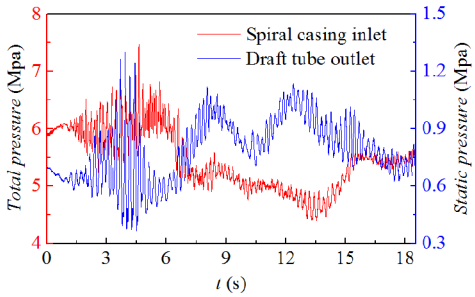

Fig. 5. Unsteady pressure at the spiral-casing inlet and the draft tube outlet.

the draft tube as shown in Fig. 5. The out flow boundary condition was used at the outlet of the clearance between the hub and the cover.

The dynamic process of closing the guide vanes was simulated according to the closing law of the guide vanes during the load rejection process in the actual pumped storage power station as shown in Fig. 6 with the dynamic mesh technology.

According to the rotor dynamics, the equation on the angular momentum balance of the rotor is defined as Eq. (1) [10]

$$M = J\frac{d\omega}{dt}, \tag{1}$$

where M is the resultant torque on the rotor, J is the inertia of the rotor, ω is the angular speed of the rotor, t is time. According to the Eq. (1), the ω_{i+1} could be obtained as shown in Eq. (2) [10].

$$\omega_{i+1} = \omega_i + \frac{M_i}{J}(t_{i+1} - t_i). \tag{2}$$

Eq. (2) was compiled into a UDF with the segregated method in C programming language. The UDF was loaded into the FLUENT software and called in each iteration time step during the unsteady flow simulation. The detailed calculation process is shown in Fig. 7. Thus, the calculation of rotational speed and flow field are coupled together.

In this paper, the transient flow in the pump-turbine during the load rejection process was initialized with the steady calculation result at the critical condition point where the pump-turbine just enters into the load rejection process.

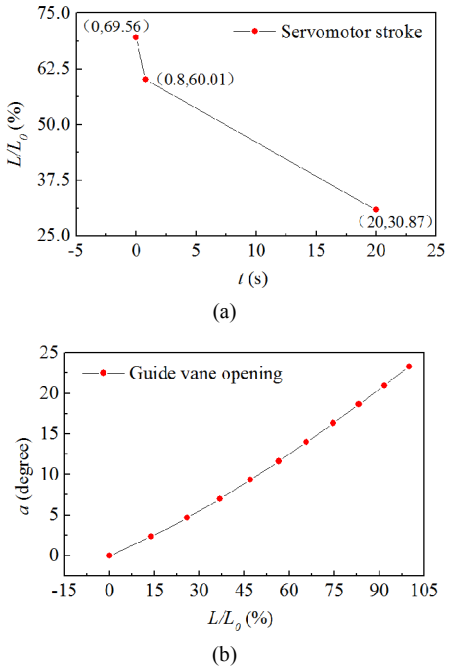

Fig. 6. Law of closing the guide vanes during the load rejection process: (a) Variation of the servomotor stroke with time; (b) relationship between the guide vane openings and servomotor stroke (L and L_0, respectively, represents the servomotor stroke and its maximum; α represents the guide vane opening).

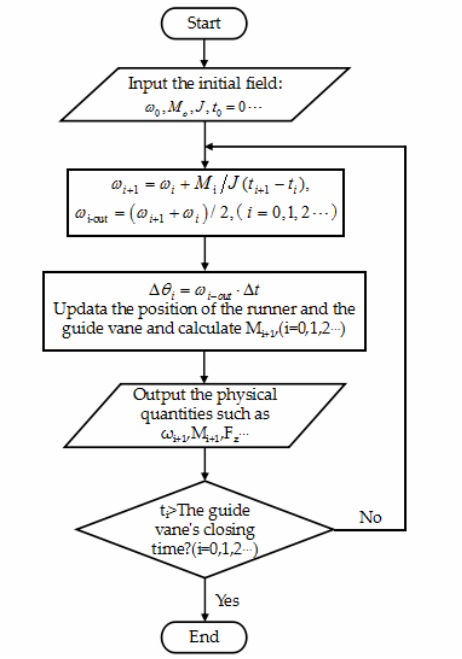

Fig. 7. Calculation procedure of the load rejection process.

2.5 Numerical schemes

In this paper, The Reynolds-averaged governing equations of turbulence were closed with the *RNG k-ε* turbulence model. The commercial flow field calculation software FLUENT based on the finite volume method (FVM) was selected to solve the closed Reynolds-averaged governing equations of turbulence. In the numerical calculation, the second-order upwind scheme was selected to discretize the convective term. Because, the under-relaxation property of the SIMPLC algorithm may accelerate convergence. The SIMPLC algorithm is more suitable for most simulations. So, it was selected to couple the pressure and velocity. Owing to the influence of the intense unsteady fluctuation characteristic of the transient flow in the load rejection process, the convergence and stability of the transient process simulation are worse than those of the normal unsteady turbulence flow simulation. But, these are natural and unavoidable for the load rejection transient process simulation. We mainly evaluated the convergence according to two methods, including the stable residuals and the consistency between the simulated performance characteristics, such as rotational speed, and those of experimental tests. The stable residuals of all the physical quantities in the numerical simulation were 10^{-5}. Different time-step sizes 0.0008 s, 0.0010 s, 0.0012 s, 0.0015 s, 0.002 s, 0.005 s and 0.008 s have even been tried to simulate the load rejection process in the first eight seconds. After tests, the time-step size 0.0012 was small enough to ensure the convergence and numerical stability of the simulation in first 18.55 seconds of the load rejection process. Therefore, the time step size 0.0012 was chosen in the unsteady simulation in this study. The maximum iteration was 25 per time step.

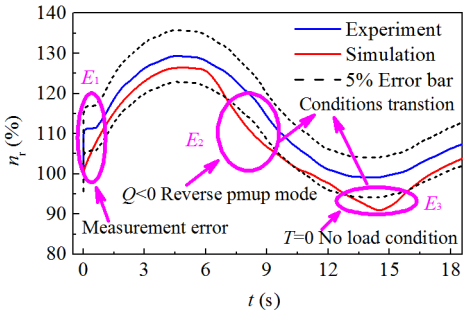

Fig. 8. Comparison between the simulated rotational speed and experimental data.

3. Results and discussion

3.1 Verification of the simulation results

To verify the accuracy of the numerical results of the load rejection process, the simulated rotational speeds were compared with the experimental data as shown in Fig. 8. The relative rotational speed is defined as Eq. (3) [10]:

$$n_r = \frac{n}{n_0} \times 100\,\%, \tag{3}$$

where n_r is the relative rotational speed, n is the transient absolute rotational speed, n_0 is the rotational speed at the initial instant of the load rejection process. Fig. 8 shows that the simulated rotational speed is basically consistent with the ex-

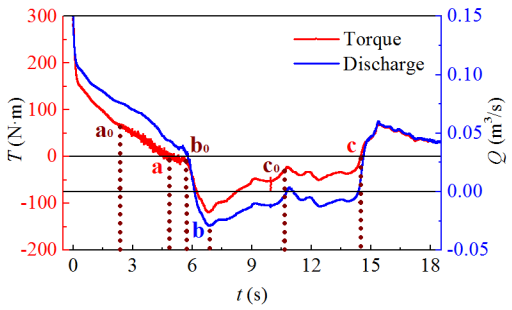

Fig. 9. Six selected typical operation conditions to analyze flow field.

perimental data on the overall trend. In most of the time of the load rejection process, the deviations between the simulated rotational speeds and the corresponding experimental data are less than 5 %. Only in the three special regions, E_1, E_2 and E_3, are the deviations more than 5 %, but less than 9 %. It is obvious that the large deviation region E_1 is mainly caused by the measurement error. In the region E_2, the pump-turbine operates near maximum reverse discharge condition of the reverse pump mode ($Q < 0$). In the region E_3, the pump-turbine operates near the no load condition ($T = 0$, namely, the hydraulic torque on the runner is zero). The maximum reverse discharge condition and the no load condition are both the critical conditions in transients. In these condition transients, the transition of the transient flow and the change of the performance characteristics are very intense. Thus, the convergence and accuracy of the simulation are not very good. Additionally, the simulated maximum relative runaway speed is 126.47 %, while the corresponding experimental value is 128.17 %. The difference between the simulated value and the experimental value is only 1.70 %. Therefore, from a global point of view, the numerical results of the transient flow are acceptable.

3.2 Analysis of the complex flow in the load rejection process

The internal and performance characteristics of a pump-turbine are closely related. The change in the performance characteristic reflects the variation of the internal flow field in a certain sense. Therefore, we selected six typical operation conditions (a, a_0, b, b_0, c and c_0) to analyze the internal flow field according to three critical operation condition points a (t = 4.8 s), b (t = 6.72 s) and c (t = 14.51 s) on the curves of discharge and hydraulic torque on the runner during the load rejection process as shown in Fig. 9. The hydraulic torque on the runner is equal to zero in the two operation conditions a (t = 4.8 s) and c (t = 14.51 s). There exists the maximum reverse discharge of the reverse pump operating process in the operation condition b (t = 6.72 s). The selected operation condition points a_0 (t = 2.4 s), b_0 (t = 5.76 s) and c_0 (t = 10.61 s) are the compared condition points, respectively, with the three critical operation condition points.

According to fluid mechanics, the criterion $\tilde{Q}$ can be used to comprehensively reflect the characteristic distribution of the velocity gradient in the flow field. It is defined as the second

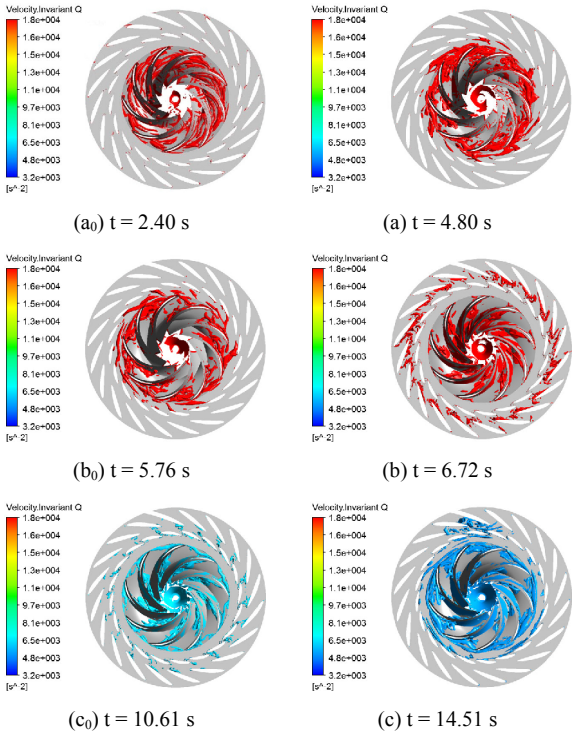

Fig. 10. Distribution of vortex core extracted with the criterion $\tilde{Q}$ in the guide/stay vanes and the runner.

invariant of the velocity gradient tensor in Eq. (4) [34-36].

$$\tilde{Q} = \frac{1}{2}(\Omega_{ij}\Omega_{ij} - S_{ij}S_{ij}), \tag{4}$$

where Ω_{ij} is the rate of rotation tensor, S_{ij} is the rate of strain tensor. The distribution of vortex core in the guide/stay vanes and the runner was extracted at six typical instants during the load rejection process according to the criterion $\tilde{Q}$ as shown in Fig. 10.

Figs. 10(a_0), (b) and (c_0) show that there are almost no vortex cores in the vaneless space at the three instants (t = 2.4 s, 6.72 s and 10.61 s), which are far away from the instants, at which the hydraulic torque on the runner equals to zero. However, Figs. 10(a), (b_0) and (c) show that there are a plenty of vortex cores in the vaneless space at the three instants (t = 4.8 s, 5.76 s and 14.51 s), that are close to the instants, at which the hydraulic torque on the runner equals zero. Fig. 10(b) shows that there are almost no vortex cores in the vaneless space at the instant (t = 6.72 s), at which the reverse discharge is maximum, under the instantaneous impact of a plenty of reverse flows during the reverse pump process, while there are more vortex cores between the guide vanes and the stay vanes.

According to its definition, it can be seen that criterion $\tilde{Q}$ reflects the combined action of vorticity and strain. Hence, the general situation of the flow in the pump-turbine during the load rejection process was analyzed above. To further analyze the complicated flow during the load rejection process in detail, the unsteady vortex flow was analyzed separately as fol-

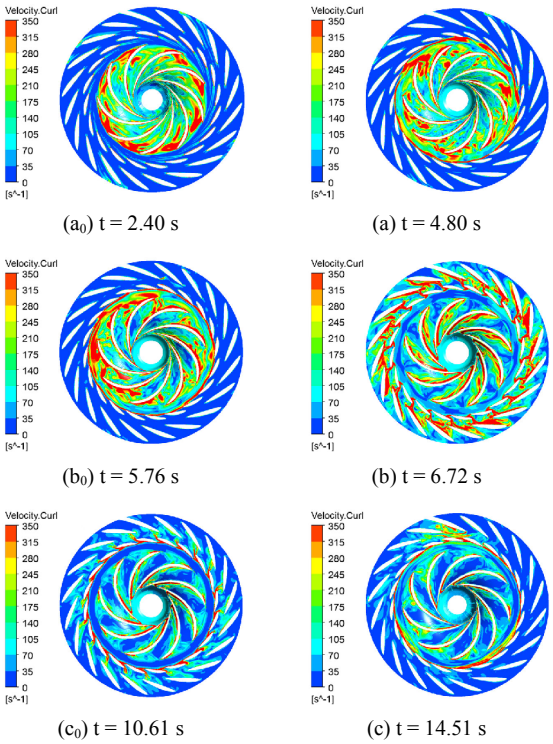

(a_0) t = 2.40 s (a) t = 4.80 s

(b_0) t = 5.76 s (b) t = 6.72 s

(c_0) t = 10.61 s (c) t = 14.51 s

Fig. 11. Magnitude distribution of vorticity in the middle-span stream surface of the guide/stay vanes and the runner.

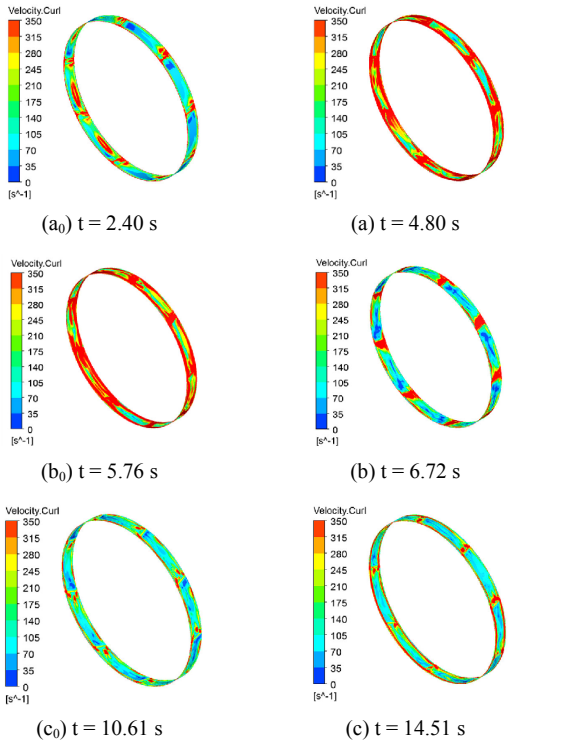

(a_0) t = 2.40 s (a) t = 4.80 s

(b_0) t = 5.76 s (b) t = 6.72 s

(c_0) t = 10.61 s (c) t = 14.51 s

Fig. 12. Magnitude distribution of the vorticity in the runner inlet torus.

lows. In fluid mechanics, the intensity of the vortex motion is generally measured with the vorticity. The vorticity is defined as the curl of the velocity as shown in Eq. (5) [32].

$$\vec{\omega} = \nabla \times \vec{v} \,, \tag{5}$$

where $\vec{\omega}$ is the vorticity vector, $\vec{v}$ is the velocity vector. The magnitude distribution of vorticity was extracted in the middle-span stream surfaces of the guide/stay vanes and the runner at different typical instants during the load rejection process as shown in Fig. 11.

Figs. 11(a_0), (b) and (c_0) show that there is almost no obvious vorticity in the vaneless space at the three instants (t = 2.4 s, 6.72 s and 10.61 s), which are far away from the instants, at which the hydraulic torque on the runner is equal to zero. However, Figs. 11(a), (b_0) and (c) show that there is significant vorticity in the vaneless space at the three instants (t = 4.8 s, 5.76 s and 14.51 s), which are close to the instants, at which the hydraulic torque on the runner is equal to zero. It can be seen from Fig. 11(b), there is almost no obvious vorticity in the vaneless space at the instant (t = 6.72 s), at which the reverse discharge is maximum, under the instantaneous impact of plenty of reverse flows during the reverse pump process. Meanwhile, stronger vorticity between the guide vanes and stay vanes could be observed. In addition, at each typical instant, there exist some shedding wake vortices near the trailing edges of the guide vanes and stay vanes. Some flow separation vortices near the leading edges of the runner blades could be also found. The vorticity intensity of the shedding wake vortex and the flow separation vortex is strong near the three instants (t = 4.8 s, 5.76 s and 14.51 s). The vorticity intensity of the shedding wake vortex and the flow separation vortex is weak at the three instants (t = 2.4 s, 6.72 s and 10.61 s), which are far away from the instants, at which the hydraulic torque on the runner is equal to zero. It indicates that the unsteady vortex flow in the vaneless space at each typical instant during the load rejection process is related to the shedding wake vortices at the trailing edges of the guide vanes and the flow separation vortices at the leading edges of the runner blades.

To fully analyze the unsteady vortex flow in the vaneless space during the load rejection process from different directions and locations, the magnitude distribution of the vorticity in the torus at the runner inlet was extracted at each typical instant during the load rejection process as shown in Fig. 12.

Figs. 12(a_0), (b) and (c_0) show that the vorticity distribution in the torus at the runner inlet is relatively weak at the three instants (t = 2.4 s, 6.72 s and 10.61 s), while Figs. 12(a), (b_0) and (c) show that the vorticity distribution is relatively strong at the three instants (t = 4.8 s, 5.76 s and 14.51 s). Furthermore, at each typical instant, the vorticity distribution near the leading edges of the runner blades and near the cover and the bottom ring in the torus is obviously stronger than that in the middle mainstream area. It indicates that the unsteady vortex flows in the vaneless space at each typical instant during the load rejection process are also related to the flow separation vortices near the leading edges of the runner blades and near the solid walls of the cover and the bottom ring.

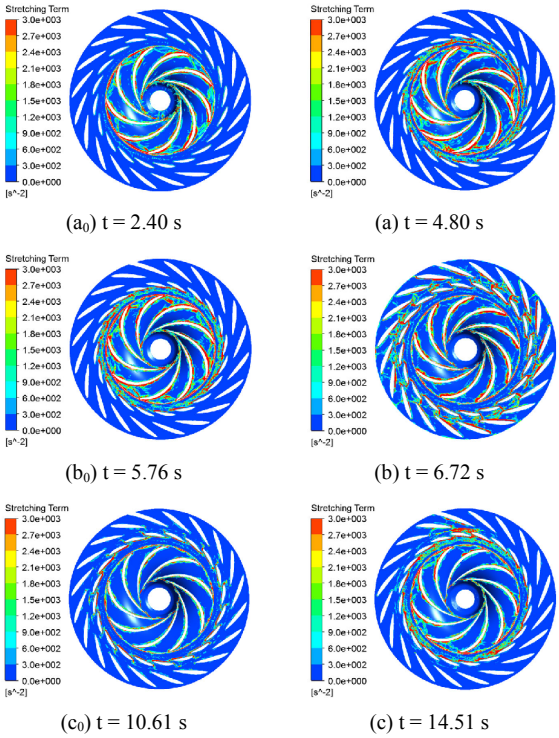

(a_0) t = 2.40 s (a) t = 4.80 s

(b_0) t = 5.76 s (b) t = 6.72 s

(c_0) t = 10.61 s (c) t = 14.51 s

Fig. 13. Magnitude distribution of $(\vec{\omega}\cdot\nabla)\vec{v}$ in the middle-span stream surface of the guide/stay vanes and the runner.

3.3 Analysis on the formation mechanism of the vortex flow

According to the above analysis, it is clear that the unsteady vortex flows in the vaneless space are related with shedding wake vortices at the trailing edges of the guide vanes and the flow separation vortices at the leading edges of the runner blades and near the solid walls of the cover and the bottom ring. The formation mechanism of the unsteady vortex flow in the vaneless space during the load rejection process was analyzed in detail as follows. For the theory of vortex dynamics, the variation of the vorticity with time for the incompressible fluid in the potential field of mass force is described with the simplified transport equation of vorticity as shown in Eq. (6) [37-39].

$$\frac{d\vec{\omega}}{dt} = (\vec{\omega}\cdot\nabla)\vec{v} + \nu\nabla^2\vec{\omega}\,, \tag{6}$$

where $(\vec{\omega}\cdot\nabla)\vec{v}$ is the stretching and twisting term of the vorticity, $\nu\nabla^2\vec{\omega}$ is the viscous diffuser term of vorticity. The magnitude distribution of the stretching and twisting term $(\vec{\omega}\cdot\nabla)\vec{v}$ was extracted in the middle-span stream surface of the guide/stay vanes and the runner at each typical instant during the load rejection process as shown in Fig. 13.

Figs. 13(a), (b_0) and (c) show that the magnitude distribution of the stretching and twisting term $(\vec{\omega}\cdot\nabla)\vec{v}$ in the vaneless space between the guide vanes and the runner at the three instants (t = 4.8 s, 5.76 s and 14.51 s) is relatively high. Thus, the primary vortex cores, including the shedding wake vortices at the trailing edges of the guide vanes and the flow separation vortices at the leading edges of the runner blades and near the solid walls of the cover and the bottom ring, are able to continually develop and evolve into the unsteady vortex flows as shown in Figs. 11(a), (b_0) and (c), under the strong enough action of the stretching and twisting of vorticity at the three instants (t = 4.8 s, 5.76 s and 14.51 s). However, Figs. 13(a_0), (b) and (c_0) show that the magnitude distribution of the stretching and twisting term $(\vec{\omega}\cdot\nabla)\vec{v}$ in the vaneless space between the guide vanes and the runners at the three instants (t = 2.4 s, 6.72 s and 10.61 s) is relatively low. Therefore, the primary vortex cores including the shedding wake vortices at the trailing edges of the guide vanes and the flow separation vortices at the leading edges of the runner blades and near the solid walls of the cover and the bottom ring are not able to continually develop and evolve into the unsteady vortex flows as shown in Figs. 11(a_0), (b) and (c_0), without the strong enough action of the stretching and twisting of vorticity at the three instants (t = 2.4 s, 6.72 s and 10.61 s). In addition, Fig. 13(b) shows that the magnitude distribution of the stretching and twisting term $(\vec{\omega}\cdot\nabla)\vec{v}$ in the vaneless space is also low at the instant (t = 6.72 s), at which the reverse discharge is maximum. But, magnitude distribution of the stretching and twisting term $(\vec{\omega}\cdot\nabla)\vec{v}$ between the guide vanes and stay vanes is high. Hence, there is almost no obvious vorticity in the vaneless space at the instant (t = 6.72 s), while there is stronger vorticity between the guide vanes and stay vanes at this instant. Corresponding stronger unsteady vortex flow between the guide vanes and stay vanes could be found at the instant (t = 6.72 s).

To analyze the effect of the viscous diffuser term $\nu\nabla^2\vec{\omega}$ on the unsteady vortex flow in the vaneless space during the load rejection process, the magnitude distribution of the viscous diffuser term $\nu\nabla^2\vec{\omega}$ was extracted in the middle-span stream surface of the guide/stay vanes and the runner at each typical instant as shown in Fig. 14. It is clear that the effect of the viscous diffuser term $\nu\nabla^2\vec{\omega}$ on the unsteady vortex flow in the vaneless space during the load rejection process is very weak. It can be neglected basically [40]. Therefore, only the stretching and twisting term $\nu\nabla^2\vec{\omega}$ was considered in this study.

In the runner inlet torus, to analyze the growth progress of the primary vortex cores, including the shedding wake vortices near the leading edges of the runner blades and the flow separation vortices near the solid walls of the cover and the bottom ring, the magnitude distribution of the stretching and twisting term $(\vec{\omega}\cdot\nabla)\vec{v}$ was extracted in the runner inlet torus at each typical instant during the load rejection process as shown in Fig. 15.

Figs. 15(a), (b_0) and (c) show that there is stronger magnitude distribution of the stretching and twisting term $(\vec{\omega}\cdot\nabla)\vec{v}$ in the runner inlet torus at the three instants (t = 4.8 s, 5.76 s and 14.51 s), which are close to the instants, at which the hydraulic torque on the runner is equal to zero. Thus, in the runner inlet torus, the primary vortex cores, including the flow

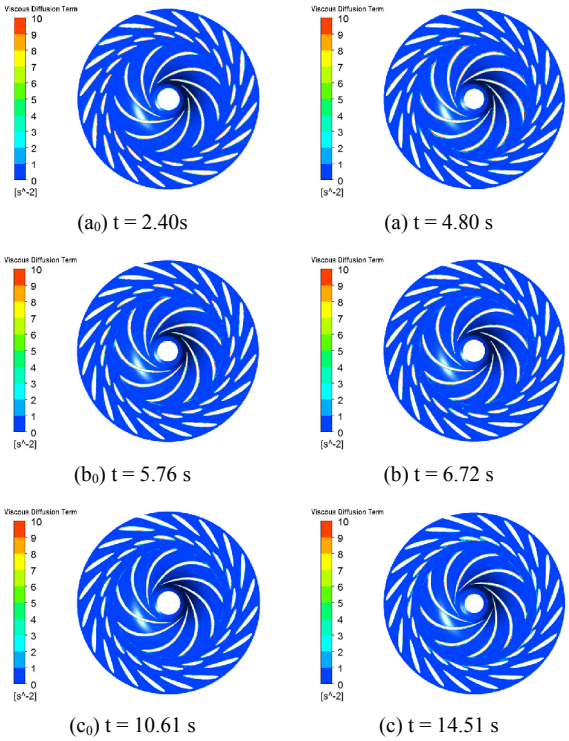

Fig. 14. Magnitude distribution of the viscous diffuser term $\nu\nabla^2\vec{\omega}$ in the middle-span stream surface of the guide/stay vanes and the runner.

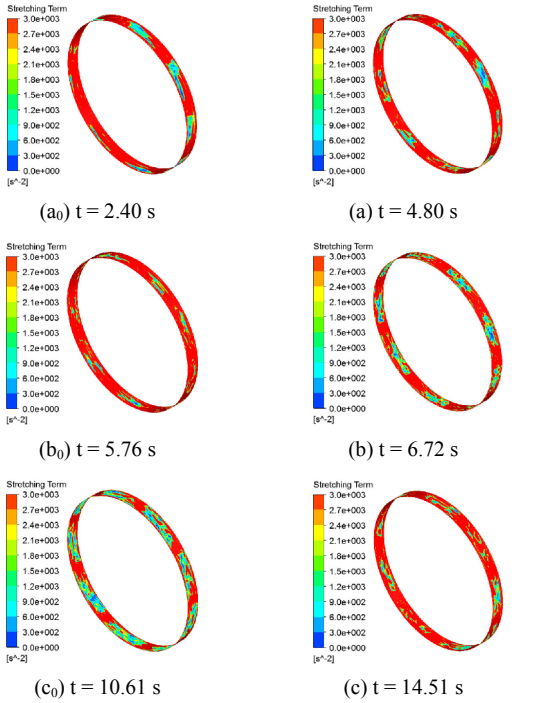

Fig. 15. Magnitude distribution of the stretching and twisting term $(\vec{\omega}\cdot\nabla)\vec{v}$ in the runner inlet torus.

separation vortices at the leading edges of the runner blades and the flow separation vortices near the solid walls of the cover and the bottom ring, are able to continually develop and evolve into the unsteady vortex flow as shown in Figs. 12(a), (b_0) and (c), under the strong enough action of the stretching and twisting of vorticity at the three instants (t = 4.8 s, 5.76 s and 14.51 s). While Figs. 15(a_0), (b) and (c_0) show that there is a weaker magnitude distribution of the stretching and twisting term $(\vec{\omega}\cdot\nabla)\vec{v}$ in the runner inlet torus at the three instants (t = 2.4 s, 6.72 s and 10.61 s). Therefore, in the runner inlet torus, the primary vortex cores, including the flow separation vortices at the leading edges of the runner blades and the flow separation vortices near the solid walls of the cover and the bottom ring, are not able to continually develop and evolve into the unsteady vortex flow as shown in Figs. 12 (a_0), (b) and (c_0), without the strong enough action of the stretching and twisting of vorticity at the three instants (t = 2.4 s, 6.72 s and 10.61 s).

In addition, according to Fig. 15, in the runner inlet torus, the magnitude distribution of the stretching and twisting term $(\vec{\omega}\cdot\nabla)\vec{v}$ near the leading edges of the runner blade and near the cover and the bottom ring is significantly higher than that in the middle mainstream zone. Therefore, in the runner inlet torus, the magnitude distribution of vorticity near the leading edges of the runner blades and near the cover and the bottom ring is higher than that in the middle mainstream zone at each typical instant during the load rejection process as shown in Fig. 12.

4. Conclusions

3-D transient turbulent flow in a pump-turbine during the load rejection process was simulated. The simulated rotational speeds were basically consistent with the corresponding experimental data. According to the numerical results, the complex flow and its formation mechanism were analyzed in detail during the load rejection process. Some conclusions were obtained as follows:

(1) There are severe unsteady vortex flows in the vaneless space near the conditions in which the hydraulic torque on the runner is equal to zero. The unsteady vortex flows in the vaneless space are mainly located near the solid walls of the cover and the bottom ring, and near the leading edges of the runner blades. When the pump-turbine operates into the maximum reverse discharge condition in the reverse pump operating process, the unsteady vortex flows in the vaneless space are instantaneously impacted into the region between the guide vanes and stay vanes by the sudden reverse flows.

(2) The unsteady vortex flows in the vaneless space originate from the primary vortex cores, under the action of the stretching, bending and twisting, near the conditions under which the hydraulic torque on the runner equals zero. The primary vortex cores consist of the shedding wake vortices of the guide vanes and the flow separation vortices near the leading edges of the runner blades and near the solid wall of the cover and the bottom ring.

In this study, the numerical results are not very ideal near the maximum reverse discharge condition (E_2 in Fig. 8) in the reverse pump mode and near the second no load condition (E_3

in Fig. 8). According to the analysis, the inaccurate turbulence model, the low qualities of the dynamic meshes and the neglected hydraulic elastic may be three relatively crucial reasons. Therefore, it is necessary to further simulate the load rejection process considering the above three factors in the future.

Acknowledgment

This work was supported by Open Fund of Key Laboratory of Fluid and Power Machinery, Ministry of Education Xihua University (Grant No. szjj2017-089 and Grant No. szjj-2017-100-1-001), and Open Research Fund Program of State key Laboratory of Hydroscience and Engineering (sklhse-2018-E-02).

Nomenclature

Q	: Discharge, $m^3 \cdot s^{-1}$
t	: Time, s
L	: Servomotor stroke, mm
L_0	: Maximum servomotor stroke, mm
a	: Guide vane opening, °
M	: Resultant torque on the rotor, N·m
J	: Inertia of the rotor, $kg \cdot m^2$
ω	: Angular speed, $rad \cdot s^{-1}$
n_r	: Relative rotational speed
n	: Rotational speed, rpm
n_0	: Rotational speed at initial instant, rpm
T	: Hydraulic torque on the runner, N·m
$\tilde{Q}$	: Second invariant of velocity gradient tensor, s^{-2}
Ω_{ij}	: Rate of rotation tensor, s^{-1}
S_{ij}	: Rate of strain tensor, s^{-1}
$\vec{\omega}$	: Vorticity, s^{-1}
$\vec{v}$	: Velocity, m s^{-1}
∇	: Hamilton operator
v	: Kinematic viscosity, m^2 s^{-1}
i	: Number of time steps

References

[1] Y. N. Zhang, T. Chen, J. W. Li and J. W. Yu, Experimental study of load variations on pressure fluctuations in a prototype reversible pump turbine in generating mode, *J. of Fluids Engineering-Transactions of the ASME*, 139 (1) (2017) 074501.

[2] X. Zhao, Y. Xiao, Z. Wang, H. Luo, A. Soo-Hwang, Y. Yao and H. Fan, Numerical analysis of non-axisymmetric flow characteristic for a pump-turbine impeller at pump off-design condition, *Renewable Energy*, 115 (2017) 1075-1085.

[3] Y. N. Zhang, Y. N. Zhang and Y. L. Wu, A review of rotating stall in reversible pump turbine, *Proceedings of the Institution of Mechanical Engineers, Part C: J. of Mechanical Engineering Science*, 231 (7) (2017) 1181-1204.

[4] D. Y. Li, H. J. Wang, Y. L. Qin, L. Han, X. Z. Wei and D. Q. Qin, Entropy production analysis of hysteresis characteristic of a pump-turbine model, *Energy Conversion and Management*, 149 (2017) 175-191.

[5] Z. G. Zuo, H. G. Fan, S. H. Liu and Y. L. Wu, S-shaped characteristics on the performance curves of pump-turbines in turbine mode – A review, *Renewable and Sustainable Energy Reviews*, 60 (2016) 836-851.

[6] D. Y. Li, H. J. Wang, Z. G. Li, T. K. Nielsen, R. Goyal, X. Z. Wei and D. Q. Qin, Transient characteristics during the closure of guide vanes in a pump-turbine in pump mode, *Renewable Energy*, 118 (2018) 973-983.

[7] D. Y. Li, H. J. Wang, Y. L. Qin, X. Z. Wei and D. Q. Qin, Numerical simulation of hysteresis characteristic in the hump region of a pump-turbine model, *Renewable Energy*, 115 (2018) 433-447.

[8] H. Zhang, D. Y. Chen, C. Z. Wu, X. Y. Wang, J. Lee and K. Jung, Dynamic modeling and dynamical analysis of pump-turbines in s-shaped regions during runaway operation, *Energy Conversion and Management*, 138 (2017) 375-382.

[9] D. Y. Li, R. Z. Gong, H. J. Wang, X. Z. Wei and D. Q. Qin, Numerical investigation on transient flow of a high head low specific speed pump-turbine in pump mode, *J. of Renewable and Sustainable Energy*, 7 (6) (2015) 63111.

[10] D. Y. Li, R. Z. Gong, H. J. Wang, G. M. Xiang, X. Z. Wei and Z. S. Liu, Dynamic analysis on pressure fluctuation in vaneless region of a pump turbine, *Science China Technological Sciences*, 58 (5) (2015) 813-824.

[11] E. Walseth, T. Nielsen and B. Svingen, Measuring the dynamic characteristics of a low specific speed pump—turbine model, *Energies*, 9 (3) (2016) 199.

[12] L. G. Zhang and D. Q. Zhou, CFD research on runaway transient of pumped storage power station caused by pumping power failure, *IOP Conf. Series: Materials Science and Engineering*, 52 (5) (2013) 52027.

[13] J. W. Li, J. Yu and Y. L. Wu, 3D unsteady turbulent simulations of transients of the francis turbine, *IOP Conf. Series: Earth and Environmental Science*, 12 (1) (2010) 12001.

[14] A. Ruprecht, T. Helmrich, T. Aschenbrenner and T. Scherer, Simulation of vortex rope in a turbine draft tube, *Proceedings of the Hydraulic Machinery and Systems 21st IAHR Symposium*, Lausanne (2002).

[15] W. D. Huang, H. G. Fan and N. X. Chen, Transient simulation of hydropower station with consideration of three-dimensional unsteady flow in turbine, *IOP Conf. Series: Earth and Environmental Science*, 15 (5) (2012) 52003.

[16] E. Casartelli, L. Mangani, O. Ryan and A. Schmid, Application of transient cfd-procedures for s-shape computation in pump-turbines with and without fsi, *IOP Conf. Series: Earth and Environmental Science*, 49 (4) (2016) 42008.

[17] X. X. Zhang and Y. G. Cheng, Simulation of hydraulic transients in hydropower systems using the 1-d-3-d coupling approach, *J. of Hydrodynamics, Ser. B*, 24 (4) (2012) 595-604.

[18] Z. J. Li, H. L. Bi, Z. W. Wang and Z. Yao, Three-dimensional simulation of unsteady flows in a pump-turbine during start-up transient up to speed no-load condition in generating mode, *Proceedings of the Institution of Mechanical Engineers Part A J. of Power & Energy*, 230 (6) (2016) 570-585.

[19] Z. J. Li, H. L. Bi, B. Karney, Z. W. Wang and Z. Yao, Three-dimensional transient simulation of a prototype pump-turbine during normal turbine shutdown, *J. of Hydraulic Research*, 55 (4) (2017) 520-537.

[20] J. Yang, G. Pavesi, S. Yuan, G. Cavazzini and G. Ardizzon, Experimental characterization of a pump – turbine in pump mode at hump instability region, *J. of Fluids Engineering*, 137 (5) (2015) 51109.

[21] W. Zeng, J. D. Yang, J. H. Hu and R. B. Tang, Effects of pump-turbine s-shaped characteristics on transient behaviours: experimental investigation, *J. of Physics: Conference Series*, 813 (1) (2017) 12056.

[22] N. Ruchonnet and O. Braun, Reduced scale model test of pump-turbine transition, *6th IAHR International Meeting of the Workgroup on Cavitation and Dynamic Problems in Hydraulic Machinery and Systems*, Ljubljana, Slovenia (2015).

[23] K. Amiri, B. Mulu, M. Raisee and M. J. Cervantes, Unsteady pressure measurements on the runner of a kaplan turbine during load acceptance and load rejection, *J. of Hydraulic Research*, 54 (1) (2016) 56-73.

[24] C. Stens and S. Riedelbauch, Cfd simulation of the flow through a pump turbine during a fast transition from pump to generating mode, *6th IAHR International Meeting of the Workgroup on Cavitation and Dynamic Problems in Hydraulic Machinery and Systems*, Ljubljana, Slovenia (2015).

[25] C. Stens and S. Riedelbauch, Investigation of a fast transition from pump mode to generating mode in a model scale reversible pump turbine, *IOP Conf. Series: Earth and Environmental Science*, 49 (2016) 112001.

[26] X. X. Zhang, Y. G. Cheng, L. S. Xia and J. D. Yang, Dynamic characteristics of a pump-turbine during hydraulic transients of a model pumped-storage system: 3d cfd simulation, *IOP Conference Series: Earth and Environmental Science,* Montreal, Canada: 2014: 22.

[27] G. Pavesi, G. Cavazzini and G. Ardizzon, Numerical analysis of the transient behaviour of a variable speed pump-turbine during a pumping power reduction scenario, *Energies*, 9 (7) (2016) 534.

[28] H. G. Fan, H. X. Yang, F. C. Li and N. X. Chen, Hydraulic torque on the guide vane within the slight opening of pump turbine in turbine operating mode, *IOP Conf. Series: Earth and Environmental Science*, 22 (032050) (2014) 1-10.

[29] Y. M. Li, G. Q. Song and Y. L. Yan, Transient hydrodynamic analysis of the transition process of bulb hydraulic turbine, *Advances in Engineering Software*, 90 (2015) 152-158.

[30] P. Côté, G. Dumas, É. Moisan and G. Boutetblais, Numerical investigation of the flow behavior into a francis runner during load rejection, *IOP Conf. Series: Earth and Environmental Science*, 22 (3) (2014) 32023.

[31] H. Hosseinimanesh, C. Devals, B. Nennemann, M. Reggio and F. Guibault, A numerical study of francis turbine operation at no-load condition, *J. of Fluids Engineering*, 139 (1) (2017) 11104.

[32] S. H. Liu, D. Q. Zhou, D. M. Liu, Y. L. Wu and M. Nishi, Runaway transient simulation of a model kaplan turbine, *IOP Conf. Series: Earth and Environmental Science*, 12 (1) (2010) 12073.

[33] E. Casartelli, L. Mangani, G. Romanelli and T. Staubli, Transient simulation of speed-no load conditions with an open-source based C++ code, *IOP Conf. Series: Earth and Environmental Science*, 22 (3) (2014) 32029.

[34] Y. N. Zhang, K. H. Liu, H. Z. Xian and X. Z. Du, A review of methods for vortex identification in hydroturbines, *Renewable and Sustainable Energy Reviews* (2017).

[35] D. Y. Li, R. Z. Gong, H. J. Wang, L. Han, X. Z. Wei and D. Q. Qin, Analysis of vorticity dynamics for hump characteristics of a pump turbine model, *J. of Mechanical Science and Technology*, 30 (8) (2016) 3641-3650.

[36] B. Ji, Y. Long, X. P. Long, Z. D. Qian, J. J. Zhou and W. X. Huai, Large eddy simulation of turbulent attached cavitating flow with special emphasis on large scale structures of the hydrofoil wake and turbulence-cavita-tion interactions, *J. of Hydrodynamics, Ser. B*, 29 (1) (2017) 27-39.

[37] X. W. Luo, A. Yu, B. Ji, Y. L. Wu and A. Y. Tsujimoto, Unsteady vortical flow simulation in a francis turbine with special emphasis on vortex rope behavior and pressure fluctuation alleviation, *Proceedings of the Institution of Mechanical Engineers Part A J. of Power & Energy*, 231 (3) (2017) 1-12.

[38] Y. Long, X. P. Long, B. Ji, W. X. Huai and Z. D. Qian, Verification and validation of urans simulations of the turbulent cavitating flow around the hydrofoil, *J. of Hydrodynamics, Ser. B*, 29 (4) (2017) 610-620.

[39] X. Long, H. Cheng, B. Ji, R. E. A. Arndt and X. Peng, Large eddy simulation and euler-lagrangian coupling investigation of the transient cavitating turbulent flow around a twisted hydrofoil, *International J. of Multiphase Flow* (2017).

[40] B. Ji, J. Wang, X. W. Luo, K. Miyagawa, L. Z. Xiao, X. P. Long and Y. Tsujimoto, Numerical simulation of cavitation surge and vortical flows in a diffuser with swirling flow, *J. of Mechanical Science and Technology*, 30 (6) (2016) 2507-2514.

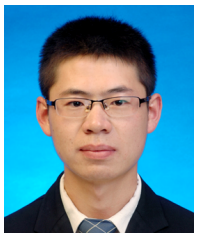

Xiaolong Fu is currently a Ph.D. candidate at School of Energy Science and Engineering, Harbin Institute of Technology, China. He obtained the Master's degree from the School of Energy Science and Engineering, Harbin Institute of Technology, China, in 2017.

Deyou Li is currently a Lecturer at School of Energy Science and Engineering, Harbin Institute of Technology, China. He received his B.S., M.S., and Ph.D. from Harbin Institute of Technology, in 2010, 2012 and 2017, respectively. His research interests include numerical simulation and experimental investigation of pump turbines, turbines and pumps.